New techniques to demodulate single image interferograms with closed fringes

Thesis presented to obtain the Doctor of Philosophy degree in Optics Sciences by

M Sc. Julio Cesar Estrada Rico

Centro de Investigaciónes en Óptica A. C.

Optics Metrology.

León Gto. México

January 23, 2008

Thesis Assessor: Dr. Manuel Servín Guirado

Contents

List of Figures

Agradecimientos

Abstract

Topics on fringe pattern demodulation, or phase recovery of interferograms, have been studied around the world by several researchers because of their importance in optical metrology areas. In our days, we can find several methods to demodulate fringe patterns, being spatial or temporal. Actually, the most used methods to recover the phase from fringe pattern images are those whose algorithms are simple and less heavy with the computer resources. For example, methods that work with interferogram images with carrier frequency either spatial or temporal, are very simple compared with methods that work with interferograms without carrier frequency, or closed fringes. Therefore, to have in some way the possibility to introduce carrier frequencies, researchers in the laboratories of optical metrology invest money in faster cameras, more powered (and pulsed) lasers and mechanical components. However, as the computer technology is advancing and is very commercial, we are able to have cheap more robust computers, in such a way that we can invest now less money in computer machines, and throw ourselves to the processing of interferograms without carrier frequency.

In this thesis, we present an original work about two new techniques to demodulate interferogram images without carrier frequency or closed fringes. Although this thesis is not a recompilation of the different demodulation methods, we start by introducing the issue of the demodulation with two simple techniques for fringe patterns with carrier frequency. The contribution of this thesis is shown in chapters 2 and 3. In chapter 2, we show an experimental method to recover the phase of interferograms with closed fringes, within a twice differentiable function space C^2. This gives a theoretical background to demodulate interferograms with closed fringes by using simple row by row scanning strategies. In chapter 3, we show a more robust method which uses robust quadrature filters. This is a very good noise-tolerant demodulation method.

Summing up, we will show how these two ideas are complemented in future works to generate temporal demodulation methods without carrier frequency. We hope forward, with this work, obtain one of the first demodulation techniques for real-time interferograms without temporal carrier frequency.

Chapter 1

Introduction

Today, with the help of digital cameras and computer aid, we can record an interferogram as digital information that can be processed numerically. An interferogram is an image with fringe patterns generated by the interference with coherent light. Without pretending to give an exhaustive exposition about light interference, let us explain, a little, how the interference fenomena is given. Suppose you have two waves:

$$U_1(P,t) = A_1(P)\exp[ik\phi_1(P) + \omega t] \tag{1.1}$$

and

$$U_2(P,t) = A_2(P)\exp[ik\phi_2(P) + \omega t], \tag{1.2}$$

where P is the spatial position, t the time position, $k = 2\pi/\lambda$ the wave number and λ its wave length, ω the angular frequency along the time and $A_1(P)$ and $A_2(P)$ the amplitudes or intensities of the wave fluctuations, respectively. We will refer to the phase functions $\phi_1(P)$ and $\phi_2(P)$ as the wave fronts of $U_1(P)$ and $U_2(P)$, respectively. Now, if these waves interfere, the result of its interference is given as its sum:

$$U(P,t) = U_1(P,t) + U_2(P,t). \tag{1.3}$$

Given the interference wave $U(P,t)$, we can obtain its amplitude or intensity $A(P)$ as

$$A(P) = U(P,t)\cdot U^*(P,t), \tag{1.4}$$

where * denotes complex conjugated. If we make some algebra we obtain that the amplitude $A(P)$ is given as

$$A(P) = A_1^2(P) + A_2^2(P) + 2A_1(P)A_2(P)\cos k[\phi_1(P) - \phi_2(P)]. \tag{1.5}$$

From here, we can see that the amplitude or intensity, of the wave of interference, is a sinusoidal spatial fluctuation whose phase is given as the phase difference of the original waves.

As the light is a form of electromagnetic radiation, we can model the light propagation of two coherent sources, as the propagation of two waves like the shown in Eq. (1.1) and (1.2). Then the light interference is given exactly as in Eq. (1.3). As our eyes are sensitive to the amplitude or the intensity of the visible electromagnetic radiation, as a result of the light interference, our eyes see the image of the spatial intensity fluctuation shown in Eq. (1.5).

This image is called interferogram or fringe pattern. In our context, more properly written, we found Eq. (1.5) closed to the following equation:

$$I(P) = a(P) + b(P)\cos k[\phi_1(P) - \phi_2(P)], \tag{1.6}$$

where $a(P) = A_1^2(P)+A_2^2(P)$ models the background illumination and $b(P) = 2A_1(P)A_2(P)$ its contrast[1].

The wave nature of light is highly exploited in optical metrology. As we can see in Eq. (1.6), the interferogram's phase is given as the difference of the wave fronts from the light sources, thus, if we take a reference light source with known wave front, we can recover the shape of the other wave front by demodulating the interferogram's image. As the wave front changes depending on the spatial distribution of the source or the medium it passes over, the interferogram's phase takes different meanings. For example, in an interferometry system

[1]For a complete and exhaustive treat about light interference, reader can consult the book of Born and Wolf [1999].

for mechanical analysis the wave front has information about stress, surface deformations or surface profiles. Hence, it is very important to develop techniques to recover the phase given a fringe pattern or interferogram if we want to recover the information of interest. Attending to this necessity, researchers in computer and optical sciences, have developed demodulation techniques since the 80's decade [Bruning et al., 1974, Takeda et al., 1982, Schwider et al., 1983, Kreis, 1986, Hariharan et al., 1987]. Now, these techniques are the basic theory of the interferogram image demodulation.

The demodulation process of an interferogram becomes simple if we have the possibility to introduce a carrier frequency either spatial or temporal. For this reason reason, researchers in optical metrology design their interferometers in such a way that, it is possible to introduce a carrier frequency in some way. However, the design of interferometers able to introduce carrier frequencies are more complicated, because they need special mounts and more sophisticated optical components such as high resolution cameras and powered lasers. This drawback, if we can call it in this way, is insignificant when the research of optical metrology has the money to invest in such a components. However, the investment may become considerably high if we work, for example, with transient or dynamic events where it is very difficult to introduce a carrier frequency. In this situations, it is better and cheaper to deal with a single image interferogram without carrier frequency or closed fringes, although the demodulation methods for closed fringes, in our days, are more complicated than those methods for open fringes or with carrier frequency. Maybe, this is the mean reason the researchers in optical metrology always look for alternatives to the introduction of carrier frequencies regardless the complexity of the optical setup.

Now, let us to introduce two techniques to demodulate iterferogram's images with carrier frequency. This kind of techniques used when we have a frequency carrier either spatial or temporal. They are very simple and not time consuming in computer implementations.

1.1 The Fourier transform method

The Fourier Transform Method (FTM) was first shown by Takeda et al. [1982]. This method works with a single fringe pattern with spatial carrier frequency. To explain this method, we first will define the mathematical model of a fringe pattern with carrier in the following way:

$$I(x,y) = a(x,y) + b(x,y)\cos[\Phi(x,y) + (u,v)\cdot(x,y)], \tag{1.7}$$

where $a(x,y)$ is a low frequency signal and, as we said before, represents the background illumination of the interferogram, $b(x,y)$ is the modulation or interference term, also known as the contrast of the image interferogram as we said before, $\Phi(x,y)$ is the phase that we want to recover, and the vector (u,v) is the induced carrier frequency in direction x and y.

To simplify the development of the FTM, let us define an interferogram with carrier just in the x direction. Then, our interferogram is

$$I(x,y) = a(x,y) + b(x,y)\cos[\Phi(x,y) + u_0 x], \tag{1.8}$$

where u_0 is the carrier frequency in x direction. This equation, using complex notation, can be simply expressed as a linear combination in the following way:

$$I(x,y) = a(x,y) + c(x,y)e^{iu_0x} + c^*(x,y)e^{-iu_0x},$$

where coefficients $c(x,y)$ and $c^*(x,y)$ are

$$c(x,y) = \frac{b(x,y)}{2}\exp[i\Phi(x,y)]$$

and

$$c^*(x,y) = \frac{b(x,y)}{2}\exp\left[-i\Phi(x,y)\right].$$

Given this, taking the linear and shifting properties of the Fourier transform, we can represent the Fourier transform of (1.8) with the following expression:

$$H(u,v) = A(u,v) + C(u-u_0,y) + C^*(u+u_0,y), \tag{1.9}$$

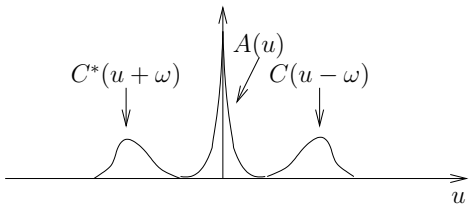

Fig. 1.1: Graphical Illustration of the Fourier transform of an interferogram with carrier frequency in x direction. (see Eq. (1.8)).

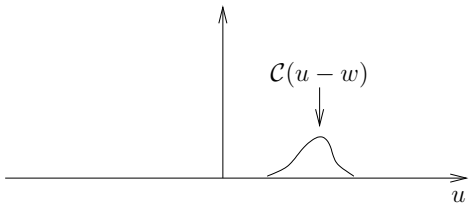

Fig. 1.2: Here we show the graph of lobe $C(u-u_0,v)$ after the filtering.

where $A(u,v)$ is the Fourier transform of $a(x,y)$, $C(u-u_0,v)$ the Fourier transform of $c(x,y)e^{iu_0x}$ and $C^*(u+u_0,v)$ the Fourier transform of $c^*(x,y)e^{-iu_0x}$. we can see a graphical illustration of this function in Fig. 1.1. The term $A(u,v)$ is centered at the origin since it is considered to be a low-frequency signal. The symmetrical lobes located around the origin, represent the Fourier spectrum of the interference term $b(x,y)\cos[\Phi(x,y)+u_0x]$. In this form, it is very easy to recover the phase of an interferogram if we filter one of the lobes, $C(u-u_o,v)$ or $C^*(u-u_o,v)$, in the Fourier space. If we filter the lobe $C(u-u_o,v)$, the Fourier spectrum graphically looks as in Fig. 1.2. 1.2. If we return to the space (x,y), assuming we have filtered the lobe $C(u-u_o,v)$, we obtain the following complex image interferogram

$$g(x,y)=c(x,y)e^{iu_0x}, \tag{1.10}$$

then, the phase is easily recovered by taking the argument of $g(x,y)e^{-iu_0x}$ as:

$$\Phi(x,y)=\arctan\left[\frac{Im\{g(x,y)e^{-iu_0x}\}}{Re\{g(x,y)e^{-iu_0x}\}}\right]. \tag{1.11}$$

Thus, given an interferogram with frequency carrier, like that of Eq. (3.2), we can easily recover its phase $\Phi(x, y)$ by using (1.11) after filtering properly the interferogram in the Fourier space.

1.2 Phase stepping interferometry

The Phase Stepping Interferometry methods (PSI), are methods to demodulate a sequence of image interferograms with temporal carrier frequency. These kind of methods are also called asynchronous temporal methods, because here we obtain the phase of each pixel in the interferogram's image independently of the others pixels[2].

These techniques are really very fast to obtain the phase of the interferogram sequence, hence, there is a lot of analysis about them. Among works treating PSI techniques, we can mention those developed by Bruning et al. [1974], Hariharan et al. [1987] and Schwider et al. [1983]. Here we are going to introduce the PSI techniques from the point of view of least square problems.

Consider an interferogram image sequence given by the following expression:

$$I(x, y, t) = a(x, y) + b(x, y)\cos(\Phi(x, y) + \omega t + \alpha), \tag{1.12}$$

where ω is the known temporal carrier frequency and α is an initial piston phase. The objective is to recover the phase given a sequence of time spaced image interferograms $t_1, t_2, t_3, \ldots, t_n$, with $n \geq 3$. With the help of trigonometric identities, we can rewrite Eq. (1.12) as

$$\hat{I}(x, y, t) = a(x, y) + C(x, y)\cos(\omega t + \alpha) + S(x, y)\sin(\omega t + \alpha), \tag{1.13}$$

[2]Strictly speaking, the Fourier transform method is also asynchronous because the phase in each pixel is obtained independently of the other pixels, however, in literature it is more common refer to the PSI techniques as asynchronous methods.

where

$$\begin{aligned} C(x,y) &= b(x,y)\cos[\Phi(x,y)] \\ S(x,y) &= -b(x,y)\sin[\Phi(x,y)]. \end{aligned} \tag{1.14}$$

Thus, it is easy to see that if we can estimate the coefficients given in (1.14), we can determine the interferogram's phase as follow:

$$\Phi(x,y) = \arctan\left[-\frac{S(x,y)}{C(x,y)}\right]. \tag{1.15}$$

Then, we translate the problem of the phase retrieval, to a problem of least squares. In this way, given an observed sequence modeled as in (1.12), we want to estimate coefficients $a(x,y)$, $C(x,y)$ and $S(x,y)$, that best fit the observation for each site (x,y). Then, in the sense of least squares, we may define the error of our estimation as:

$$E[a(x,y), C(x,y), S(x,y)] = \sum_{n=1}^{N} \left\{a(x,y) + C(x,y)\cos(\omega t_n + \alpha) + S(x,y)\sin(\omega t_n + \alpha) - I(x,y,t_n)\right\}^2, \tag{1.16}$$

therefore, we must to minimize this error in order to obtain the coefficients $a(x,y)$, $C(x,y)$ and $S(x,y)$.

To minimize the quadratic error given by (1.16), we take its derivatives with respect to each coefficient $[a(x,y), C(x,y), S(x,y)]$ and we equal these to zero, in such a way that we obtain the following linear equation system

$$\begin{pmatrix} N & \sum\cos(\omega t_n+\alpha) & \sum\sin(\omega t_n+\alpha) \\ \sum\cos(\omega t_n+\alpha) & \sum\cos^2(\omega t_n+\alpha) & \sum\cos(\omega t_n+\alpha)\sin(\omega t_n+\alpha) \\ \sum\sin(\omega t_n+\alpha) & \sum\cos(\omega t_n+\alpha)\sin(\omega t_n+\alpha) & \sum\sin^2(\omega t_n+\alpha) \end{pmatrix} \cdot \begin{pmatrix} a(x,y) \\ C(x,y) \\ S(x,y) \end{pmatrix} = \begin{pmatrix} \sum I(x,y,t_n) \\ \sum I(x,y,t_n)\cos\omega(\omega t_n+\alpha) \\ \sum I(x,y,t_n)\sin\omega(\omega t_n+\alpha) \end{pmatrix}. \tag{1.17}$$

Then, we must to solve this linear equation system in order to obtain coefficients $a(x,y)$, $C(x,y)$ and $S(x,y)$.

Summing up, this is the general procedure to estimate coefficients $C(x,y)$ and $S(x,y)$, in order to recover the phase from an image interferogram set with known temporal carrier frequency. In theory, each interferogram set may have any time separation between interferograms [Greivenkamp, 1984]. However, taking into account the work presented by Morgan [1982], if we consider that the time separation between interferograms is constant and the interferograms are uniformly distributed into k periods of the temporal signal, we can define the temporal carrier frequency in the following way:

$$\omega = \frac{2\pi k}{N\Delta t}, \tag{1.18}$$

where k is the number of periods for the temporal signal, Δt the time separation between each interferogram and N the number of interferograms. In Fig. 1.3, we illustrate how the interferogram sequence is located in one period of the temporal signal. The left graphic shows the interferogram separation for a temporal carrier of $\omega = 2\pi/3$, while the right shows the interferogram separation for a temporal carrier of $\omega = \pi/2$. In both cases, the initial piston phase is $\alpha = 0$, and the time separation is $\Delta t = 1$.

For the cases as that are shown in Fig. 1.3, when the interferograms are uniformly spaced into one period of the temporal signal and the time separation is $\Delta t = 1$, we see that the temporal carrier frequency is given as:

$$\omega = \frac{2\pi}{N},$$

where N is the number of interferograms. If this is the case, then we can obtain the following:

$$\sum_{n=1}^{N} \cos\left(\frac{2\pi}{N}n + \alpha\right) = 0, \qquad \sum_{n=1}^{N} \sin\left(\frac{2\pi}{N}n + \alpha\right) = 0. \tag{1.19}$$

On the other hand, as the cosine is the sine quadrature[3] and viceversa, its inner product is zero, therefore we have the following too:

$$\sum_{n=1}^{N} \cos\left(\frac{2\pi}{N}n + \alpha\right) \sin\left(\frac{2\pi}{N}n + \alpha\right) = 0. \tag{1.20}$$

[3]This is that the cosine function is orthogonal to the sine function

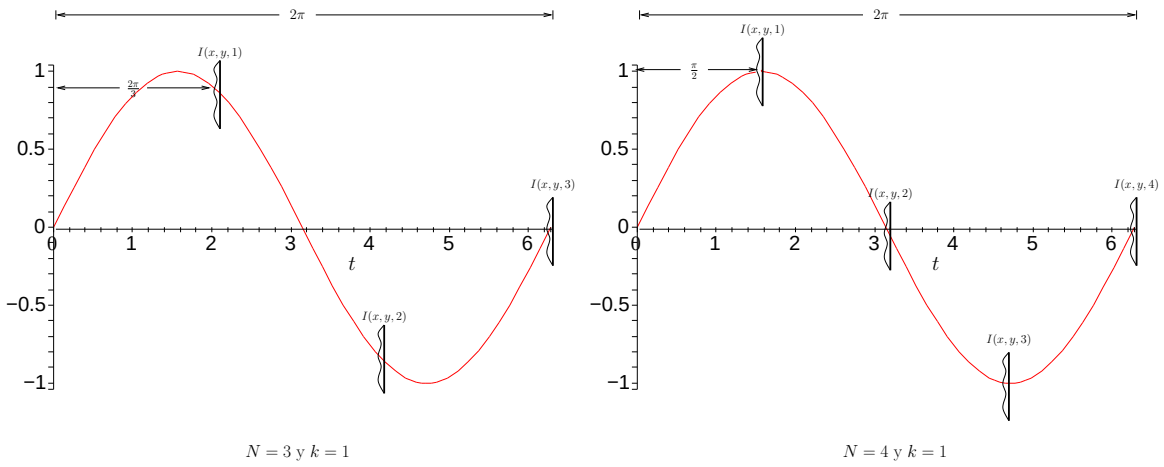

Fig. 1.3: An interferogram sequence located in one period a temporal signal. In the left, we see the position of interferograms for $N = 3$ and $\omega = 2\pi/3$ and the right show the position of interferograms for $N = 4$ and $\omega = \pi/2$. The initial piston phase is $\alpha = 0$ in both cases. The time interval is $\Delta t = 1$.

Using trigonometric identities again, we can have the following relations as well:

$$\sum_{n=1}^{N} \cos^2\left(\frac{2\pi}{N}n + \alpha\right) = \frac{N}{2}, \qquad \sum_{n=1}^{N} \sin^2\left(\frac{2\pi}{N}n + \alpha\right) = \frac{N}{2}. \tag{1.21}$$

For this particular case, the equation system shown in expression (1.17) is simplified having just the following form:

$$\begin{pmatrix} N & 0 & 0 \\ 0 & \frac{N}{2} & 0 \\ 0 & 0 & \frac{N}{2} \end{pmatrix} \begin{pmatrix} a(x,y) \\ C(x,y) \\ S(x,y) \end{pmatrix} = \begin{pmatrix} \sum I(x,y,n) \\ \sum I(x,y,n)\cos\left(\frac{2\pi}{N}n + \alpha\right) \\ \sum I(x,y,n)\sin\left(\frac{2\pi}{N}n + \alpha\right) \end{pmatrix}, \tag{1.22}$$

where we have done a change of variable from t_n to n in order to simplify the notation. The sums go from $n = 1$ until N. Then, we can see that coefficients $a(x, y)$, $C(x, y)$ and $S(x, y)$

are determined by solving (1.22) as follow:

$$a(x,y) = \frac{1}{N}\sum_{n=n}^{N} I(x,y,n), \tag{1.23}$$

$$C(x,y) = \frac{2}{N}\sum_{n=n}^{N} I(x,y,n)\cos\left(\frac{2\pi}{N}n+\alpha\right), \tag{1.24}$$

$$S(x,y) = \frac{2}{N}\sum_{n=n}^{N} I(x,y,n)\sin\left(\frac{2\pi}{N}n+\alpha\right). \tag{1.25}$$

And finally, once we have the coefficients estimated, we can recover the phase as

$$\Phi(x,y) = \arctan\left(-\frac{\sum I(x,y,n)\sin\left(\frac{2\pi}{N}n+\alpha\right)}{\sum I(x,y,n)\cos\left(\frac{2\pi}{N}n+\alpha\right)}\right). \tag{1.26}$$

The importance of this result is that to estimate coefficients $C(x,y)$ and $S(x,y)$ we only have to take N equally time spaced interferograms using the following temporal carrier frequency:

$$\omega = \frac{2\pi}{N},$$

being N the number of interferograms to be taken. We can adjust an initial piston phase α to help us analytically simplify the phase recovery. For example, if we adjust an initial piston phase $\alpha = -\pi/3$, for $N = 3$, then our temporal carrier will be $\omega = 2\pi/3$, and our first interferogram will be taken on position $\pi/3$ and the next two on positions π and $5\pi/3$ respectively, according to our temporal carrier frequency ω. In this particular case where $N = 3$ and $\alpha = -\pi/3$, it is easy to see that the phase is determined as:

$$\Phi(x,y) = \arctan\left(\frac{-\sqrt{3}[I(x,y,1) - I(x,y,3)]}{I(x,y,1) - 2I(x,y,2) + I(x,y,3)}\right), \tag{1.27}$$

replacing values directly in Eq. (1.26).

1.3 Summary

A we may see, the techniques developed in 80's decade, to demodulate image interferograms, were developed assuming that the interferograms have an spatial or temporal carrier frequency. However, there is some circumstances where it is impossible to introduce a carrier

frequency, spatial or temporal, due to the nature of the experiment. For this reason, our interest is to demodulate single image interferograms with closed fringes, or in other words, without carrier frequency. One of the first intents to demodulate a single image interferogram with closed fringes was made by Kreis [1986], by using the Hilbert transform. However, until Servin et al. [1997] was defined a more robust demodulation method for single fringe patterns with closed fringes.

In the next chapters we will show two works to demodulate single fringe patterns with closed fringes, these works are part of our original work reported in [Estrada et al., 2006, 2007].

Chapter 2

Path independent demodulation within the function space C^2

As we said in the last chapter, there are several works around the world, already published, about demodulating *Single Fringe Pattern Images* (SFPI) with closed fringes. The two better known methods are the *regularized phase tracker* (RPT), and the *two-dimensional Hilbert Transform* method (2D-HT). In both cases, the demodulation success depends strongly on the path followed to obtain the expected estimation. Therefore, both RPT and 2D-HT are path dependent methods. Here, we will show a novel method to demodulate SFPI with closed fringes which may follow arbitrary sequential paths. Through the work presented here, we introduce a new technique to demodulate SFPI with estimations within the function space C^2; in other words, estimations where the phase curvature is continuous. The technique developed here, uses a frequency estimator which searches into a frequency discrete set. It uses a second order potential regularizer to force the demodulation system to look into the function space C^2. The obtained estimator is a fast demodulator system for normalized SFPI with closed fringes. Some tests to demodulate SFPI with closed fringes using this technique following arbitrary paths are presented. The results are compared to those from RPT technique. Finally, an experimental normalized interferogram is demodu-

lated with the herein suggested technique[1].

2.1 Introduction

Applications of optical interferometry in areas such as digital contouring or strain analysis in mechanics are very important because they are non-invasive techniques and give full field measurements [Mujeeb et al., 2006]. For example, the *electronic speckle pattern interferometry* technique (ESPI), is widely used in this areas [Butters and Leendertz, 1971]. As the information of interest is usually phase modulated in the generated image interferogram, it is necessary to apply a demodulation technique.

A Single Fringe Pattern Image (SFPI) is an image interferogram that is considered as a sinusoidal two-dimensional signal (without taking random fluctuations into account) given by the following function:

$$I(x, y) = a(x, y) + b(x, y)\cos[\phi(x, y)], \tag{2.1}$$

assuming that $a(x, y)$ and $b(x, y)$ are continuous smooth functions. (x, y) are integer values that represent a site on the image lattice L where the interferogram is recorded. However, here we assume that we are working with a normalized fringe pattern as the following:

$$I'(x, y) = \cos[\phi(x, y)]. \tag{2.2}$$

There are several fringe pattern normalization techniques. For example, Quiroga and Servin [2003] uses an isotropic fringe pattern normalization, while Guerrero et al. [2005] uses monogenic filtering for the fringe pattern normalization.

The demodulation process is based on recovering the encoded phase $\phi(x, y)$ given the fringe pattern image. To do this, the only information we have are the intensity values $I(x, y)$ of the fringe pattern. When it is possible to introduce a carrier frequency while the

[1] See Ref. [Estrada et al., 2006]

fringe pattern image is being recorded, the modulating phase is given as:

$$\phi(x, y) = \phi_0(x, y) + \omega x, \tag{2.3}$$

where ω is the introduced spatial carrier frequency in x direction. In this case, the modulating phase is recovered by the well known Fourier transform methods [Takeda et al., 1982]. However, when non repetitive transitory phenomena are being analyzed, based on speckle interferometry systems, it is usually impossible to introduce a carrier frequency, be it spatial or temporal [Stetson and Brohinsky, 1988, Bruning et al., 1974]. In these cases, there is no choice but to deal with a SFPI with closed fringes.

Two methods that have marked the way to demodulate SFPI with closed fringes are the *Regularized phase tracker* (RPT) by Servin *et. al.* Servin et al. [2001] and the *two-dimensional Hilbert Transform* method (2D-HT) by Larkin *et. al.* [Larkin et al., 2001]. 2D-HT defines the following vortex operator to obtain the interferogram's quadrature in order to demodulate it:

$$\mathcal{V}(I) = -i \exp(-i\beta_{2\pi})\mathcal{F}^{-1}\{\exp(i\psi)\mathcal{F}\{I\}\}, \tag{2.4}$$

where $\mathcal{F}$ denotes the 2D Fourier transform. Then, the modulating phase is obtained as follow:

$$\hat{\phi}(x, y) = \arctan\left[\frac{\mathcal{V}[I(x, y)]}{I(x, y)}\right]. \tag{2.5}$$

The term $\beta_{2\pi} = \beta_{2\pi}(x, y)$ in Eq. (2.4) is the modulo 2π fringe pattern's orientation field and may be defined as follow:

$$\beta_{2\pi}(x, y) = \arctan\left[\frac{\partial\phi(x, y)/\partial y}{\partial\phi(x, y)/\partial x}\right]. \tag{2.6}$$

Function $\exp[i\psi(u, v)]$ is called an spiral phase function given by the following expression:

$$\exp[i\psi(u, v)] = \frac{u + iv}{\sqrt{u^2 + v^2}} \tag{2.7}$$

As we can see in Eq. (2.4), we need to have the fringe orientation field $\beta_{2\pi}(x, y)$ in order to use the vortex operator (2.4). Eq. (2.6) looks very easy to compute, but we

obviously do not have access to the phase of the interferogram. Instead, we have access to the interferogram's image and we have to estimate the orientation field $\beta_{2\pi}(x, y)$ modulo 2π given the interferogram's image. However, to estimate the fringe orientation field $\beta_{2\pi}(x, y)$ from the image interferogram is almost as difficult as to estimate the phase using RPT method. Larkin *et. al.* suggested this quadrature operator in Ref. Larkin et al. [2001], but in their paper it is not presented how to obtain the fringe orientation field. However, in Ref. Larkin [2001], an outline of the orientation estimation problem was given and in Ref. Larkin [2005] a way is proposed to obtain the orientation field. Another approach, previous to the work of Larkin, to obtain the modulating phase, based on the orientation field of the fringe pattern, was given in Ref Marroquin [1998], which propose a regularized strategy to obtain the orientation field to correct the sign changes in the phase obtained by the Hilbert transform.

Quiroga *et. al.* Quiroga et al. [2002] and Villa *et. al.* Villa et al. [2005] proposed separate sequential methods for the fringe orientation field estimation. For example, in Ref. Villa et al. [2005] a linear orientation field estimator for $\beta_{2\pi}(x, y)$ is proposed that works minimizing sequentially along the fringes the next cost functional with respect to $n(x, y) = [n_x(x, y), n_y(x, y)]$ at each site (x, y):

$$U[n(x,y)] \quad = \quad \sum_{(\eta,\xi)\in\Gamma_{x,y}} \left\{ \|\nabla I'(\eta,\xi)\cdot n(\eta,\xi)\|^2 \, - \, \|n(\eta,\xi) - n_0(\eta,\xi)\|^2 s(\eta,\xi) \right\}, \quad (2.8)$$

where $s(\eta, \xi)$ is a function indicator that is 1 if the vector $n_0(\eta, \xi)$ was already estimated previously and 0 in other case. When is estimated the vector $n(x, y)$, by minimizing (2.8), is set $s(x, y) = 1$ to label the vector $n(x, y)$ as estimated. The operator $\nabla(\cdot)$ is the gradient operator. Here is assumed that the interferogram $I'(x, y)$ is filtered with a high pass filter, in such a way that $I'(x, y)$ can be represented as

$$I'(x, y) = b(x, y)\cos[\phi(x, y)]$$

. Once the normalized vector field $n(x, y)$ is estimated, the orientation field, module 2π, is

obtained as:

$$\hat{\beta}_{2\pi}(x,y) = \arctan\left[\frac{n_y(x,y)}{n_x(x,y)}\right]. \tag{2.9}$$

On the other hand, RPT which has inspired all the fringe following sequential methods, obtains the interferogram's phase by minimizing the following cost functional with respect to $\hat{\phi}(x,y)$, ω_x and ω_y at the site (x,y):

$$\begin{aligned} U[\hat{\phi}(x,y),\omega_x,\omega_y] \quad = \quad & \sum_{(\eta,\xi)\in\Gamma_{x,y}} \Big\{[cos[P(x,y,\eta,\xi)] - I'(\eta,\xi)]^2 \\ & + \lambda[\hat{\phi}(\eta,\xi) - P(x,y,\eta,\xi)]^2 s(\eta,\xi)\Big\}, \end{aligned} \tag{2.10}$$

where $P(x,y,\eta,\xi) = \hat{\phi}(x,y) + \omega_x(x-\eta) + \omega_y(y-\xi)$ is a phase plane that fits the observed data in neighborhood $\Gamma_{x,y}$ around the site (x,y), $I'(x,y)$ is the normalized observed data given by (2.2), the second term is called the regularization term and is as a low-pass filter term, being thus the RPT method robust under certain conditions of noise, $\lambda > 0$ is as the bandwith of the regularization term. The function $s(\eta,\xi)$ is a function indicator that is 1 if phase was already estimated in site (η,ξ), and 0 in other case. In both cases (Eq. 2.8 and 2.10) the estimation process starts at a site (x,y) which is the initial seed that is sequentially propagated along a sequential path on the image interferogram.

The minimization process for Eq. (2.8) and (2.10) is difficult and depends strongly on the initial seed given and on the path followed during the SFPI demodulation. These methods are called path dependent since from all the possible paths to follow in the two-dimensional interferogram's space, only the path following the fringes yields the expected phase. To illustrate this, in Fig. 2.1, we see two global solutions given for the same SFPI following different paths with the RPT. In the panel labeled *Wrong phase*, we see a phase estimation following an arbitrary path, while in the panel labeled *Expected phase*, we see a phase estimation following the fringes, making the path dependence of the RPT evident.

In this thesis, we propose a novel idea, which constrains the phase estimation to look into the function space C^2; that is, estimated phases with a continuous phase curvature. With

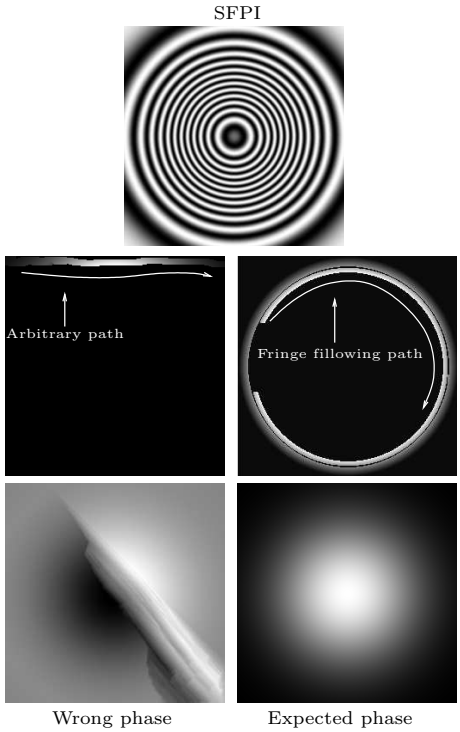

Fig. 2.1: Two estimated phases using the RPT from the same SFPI given. Panel labeled *Wrong phase* shows the obtained phase by following an arbitrary path, while panel labeled *Expected phase* is obtained using a fringe following path. The SFPI given is in panel labeled *SFPI*.

this restriction we remove the local ambiguities avoiding wrong solutions as that shown in Fig. 2.1 in the panel labeled *Wrong phase*. Searching into this function space C^2, we obtain the expected modulated phase regardless of the path followed by the demodulator. Our technique consists in developing a local frequency estimator with second order regularizer potentials to obtain the expected phase $\hat{\phi} \in C^2$. This frequency estimator searches the expected frequency into a discrete frequency set. In the next section, we will develop the local frequency estimator and we will show how to obtain the phase given the estimated local frequency for each site in the image interferogram. Also, we are going to show with examples, that the technique developed is path independent and obtains the expected modulating phase.

2.2 Method

Let's assume first a one-dimensional space x. Then our normalized fringe pattern looks like:

$$I'(x) = \cos[\phi(x)]. \tag{2.11}$$

To avoid ambiguities in the demodulation process, we limit the estimator's degrees of freedom by restricting the demodulated phase ϕ to the set C^2 of twice differentiable functions. With this in mind, we start proposing the phase estimation by adjusting the local frequency. Then, we have the following relation:

$$\cos[\hat{\phi}(x) + \omega(x)(x - x_+)] \approx I'(x_+), \tag{2.12}$$

the modulating phase $\hat{\phi}(x) + \omega(x)(x - x_+)$ is a first order Taylor expansion around site x of the actual phase $\phi(x)$, where $\hat{\phi}(x)$ is already known previously and $\omega(x) = \mathtt{d}\phi(x)/\mathtt{d}x$ is the local frequency between x and x_+. $I'(x)$ is the normalized signal (Eq. 2.11). Site x_+ is such that may take the following values:

$$x_+ = \begin{cases} x - 1 & \texttt{left} \\ x + 1 & \texttt{right} \end{cases} \tag{2.13}$$

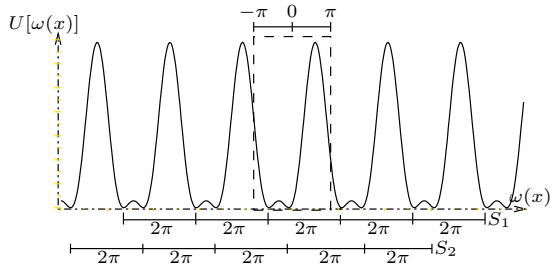

(a)

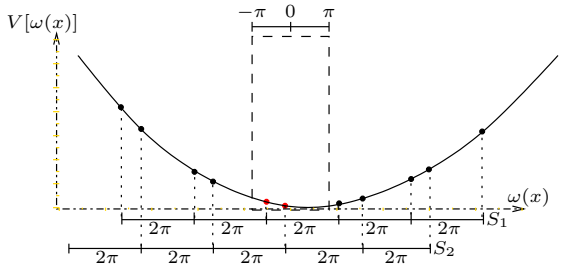

(b)

Fig. 2.2: In this figure, (a) is the graph of the cost function (2.14) and (b) is the graph of the regularizer potential (2.20). The graph (a) was generated using the parameters $I'(x) = 0.66$ and $\hat{\phi}(x) = 20$. We also show the series S_1 and S_2, which corresponds to the minimum values of the cost function (2.14). In graph (b) we see that exists only one frequency $\omega(x) \in \Omega = \{S_1, S_2\}$ that minimizes Eq. (2.20).

depending on the demodulation direction taken. We propose to minimize the following cost function to estimate the frequency $\omega(x)$ that satisfies Eq. (2.12):

$$U[\omega(x)] = \{\cos[\hat{\phi}(x) + \omega(x)(x - x_+)] - I'(x_+)\}^2. \tag{2.14}$$

In Fig. 2.2(a) we show the graph for this cost function. As shown in Fig. 2.2(a), this cost function is ambiguous since it has multiple minimum values due to the cosine periodicity. But, all the minimum values of Eq. (2.14) can be generated with the following two series:

$$S_1 = (W[\hat{\phi}(x)] - \arccos[I'(x_+)])(x - x_+) \pm 2n\pi \tag{2.15}$$

$$S_2 = (W[\hat{\phi}(x)] + \arccos[I'(x_+)])(x - x_+) \pm 2n\pi, \tag{2.16}$$

for $n = 0, 1, 2, \ldots$, where the wrapping operator $W[\cdot]$ wraps the phase $\hat{\phi}(x)$ in the interval $[-\pi, \pi]$. These series are also shown in graph 2.2(a) to see the correspondence with the minimum values.

As the maximum frequency that a fringe pattern may have in a image interferogram is π radians per pixel, we are interested on the frequencies that are in the interval $[-\pi, \pi]$. These frequencies may be taken from the series of Eq. (2.15) and (2.16) as follow:

$$\omega_1 = \begin{cases} \omega(x) & \texttt{if} \quad |\omega(x)| \leq |\pi| \\ \omega(x) - 2\pi & \texttt{if} \quad \omega(x) > \pi \\ \omega(x) + 2\pi & \texttt{if} \quad \omega(x) < -\pi \end{cases} \tag{2.17}$$

for $\omega(x) = (W[\hat{\phi}(x)] - \arccos[I'(x_+)])(x - x_+)$ and

$$\omega_2 = \begin{cases} \omega(x) & \texttt{if} \quad |\omega(x)| \leq |\pi| \\ \omega(x) - 2\pi & \texttt{if} \quad \omega(x) > \pi \\ \omega(x) + 2\pi & \texttt{if} \quad \omega(x) < -\pi \end{cases} \tag{2.18}$$

for $\omega(x) = (W[\hat{\phi}(x)] + \arccos[I'(x_+)])(x - x_+)$. Then we define the discrete set $\Omega = \{\omega_1, \omega_2\}$ as the domain of all possible frequencies that minimize (2.14) and are in the interval $[-\pi, \pi]$.

Because we want that the estimated phase $\hat{\phi}(x)$ belongs to the function space C^2, we take the *priori* assumption that the phase curvature in a site x is very smooth in its neighborhood. Then, we suggest the following potential regularizer to penalize the strong phase curvature variations between the neighbors x and $x + 1$:

$$\begin{aligned} V[\hat{\phi}(x)] &= [C_{\hat{\phi}}(x) - C_{\hat{\phi}}(x+1)]^2 \\ &= [\hat{\phi}(x-2) - 2\hat{\phi}(x-1) + \hat{\phi}(x) - \\ &\quad \hat{\phi}(x-1) + 2\hat{\phi}(x) - \hat{\phi}(x+1)]^2, \end{aligned} \tag{2.19}$$

where, as we can see in this equation, the operator $C_{\hat{\phi}}(\cdot)$ estimates the backwards phase curvature in the given site. This, in frequency terms is reduced to:

$$V[\omega(x)] = [\omega(x-2) - 2\omega(x-1) + \omega(x)]^2 \tag{2.20}$$

if we take the demodulation direction to the right and observing that $\hat{\phi}(x-2) - 2\hat{\phi}(x-1) + \hat{\phi}(x) = w(x) - w(x-1)$ and $\hat{\phi}(x-1) + 2\hat{\phi}(x) - \hat{\phi}(x+1) = w(x+1) - w(x)$. If we take the demodulation direction to the left we have

$$V[\omega(x)] = [\omega(x) - 2\omega(x+1) + \omega(x+2)]^2. \tag{2.21}$$

As we can see in Fig. 2.2(b), in the interval $[-\pi, \pi]$, this potential regularizer removes the ambiguities given by cost function (2.14) since it has only a frequency in Ω that minimizes it. Therefore, we suggest the following estimator to obtain the frequency:

$$\hat{\omega}(x) = \min_{\omega(x)\in\Omega} V[\omega(x)], \tag{2.22}$$

where the searched frequency must to be in the discrete set $\Omega = \{\omega_1, \omega_2\}$. $V[\omega(x)]$ is defined as in Eq. (2.20) or (2.21), depending on how the demodulation direction is taken. Finally we obtain the phase for the current site x_+ given by the frequency $\hat{\omega}(x)$ with the estimator of Eq. (2.22) as follows:

$$\hat{\phi}(x_+) = \hat{\phi}(x) + \hat{\omega}(x)(x - x_+), \tag{2.23}$$

which is continuous in curvature since the frequency $\hat{\omega}(x)$ obtained with estimator (2.22), gives the minimum possible phase curvature variation between the neighbors sites of x and x_+.

Eq. (2.23) have some similarity with the *Phase Locked Loop* (PLL) method applied to demodulate interferograms. In 1993, Servin Servin et al. [1994] showed the implementation of a PLL method to demodulate SFPI with carrier frequency. Their iteration to update the phase in a site $x+1$ is given as follow:

$$\hat{\phi}(x+1) = \hat{\phi}(x) - \tau[I'(x) - I'(x-1)]\sin[\phi(x) + \omega_0 x], \tag{2.24}$$

where, as we can see, there must exist a carrier frequency ω_0 in order to apply PLL method successfully. In the literature, we can find second-order PLL implementations applied to fringe patterns as that reported in Gdeisat et al. [2000], but all PLL methods works only if a

carrier frequency is given in the fringe pattern image. Therefore, there are strong differences between (2.24) and (2.23). First, the frequency for (2.23) is estimated using (2.22) in such a way that it preserves a ***continuous phase curvature*** and second, frequency estimator (2.22) is applicable to fringe pattern signals with and without carrier frequency. In contrast, PLL only assumes phase continuity.

2.2.1 Demodulation process.

The demodulation process, considering the previous development, may be summarized with the following steps:

1. Choose a site x as the initial seed to start the demodulation sequence.
2. Set the estimated phase in the initial seed as $\hat{\phi}(x) = \arccos[I'(x)]$.
3. Set the estimated phase in the initial seed neighborhood as $\hat{\phi}(x+1) = \arccos[I'(x+1)]$ and $\hat{\phi}(x-1) = \arccos[I'(x-1)]$.
4. For each subsequent site x_+ to the left and right, that isn't estimated, do the following:
   (a) Construct the frequency discrete set $\Omega = \{\omega_1, \omega_2\}$ using Eq. (2.17) and (2.18).
   (b) Take the frequency $\hat{\omega}(x)$ as shown in Eq. (2.22).
   (c) Set the estimated phase in the site x_+ using Eq. (2.23).

In this way, we have a simple and fast demodulation process that we are going to call *Frequency Curvature Tracker* (FCT) because it estimates the frequency restricting its curvature to obtain the phase in each site x.

A more robust way to set the phase in the neighborhood of the initial seed in step 3, is the following: construct the frequency set for site $x-1$ and $x+1$ and choose the frequency combination that gives less phase curvature. In other words, we use the following criteria

to choose the frequencies for sites $x-1$ and $x+1$:

$$[\hat{\omega}(x-1), \hat{\omega}(x+1)] = \min_{\substack{\omega(x-1) \in \Omega_l, \\ \omega(x+1) \in \Omega_r}} [\omega(x-1) - \omega(x+1)]^2. \tag{2.25}$$

The phase $\phi(x-1)$ and $\phi(x+1)$ is set according to Eq. (2.23), where Ω_l is the frequency discrete set to the left (site $x-1$) and Ω_r is the frequency discrete set to the right (site $x+1$). This is better than using arc cosine functions like in step 3 because the frequency around the initial seed with arc cosine functions, may abruptly change its sign.

Now, we are going to test the FCT and to campare it with the RPT applied to the one-dimensional case to observe that the obtained phase $\hat{\phi}$ with the FCT is $\hat{\phi} \in C^2$. Let us demodulate the signal showed in 2.3(a) which its modulating phase is modeled as $\phi(x) = \frac{1}{2}ax^2$. In Fig. 2.3(b) we see the phase obtained with the FCT technique and Fig. 2.3(d) shows its phase curvature. In Fig. 2.3(c) we see the phase obtained with the RPT technique and Fig. 2.3(e) shows its phase curvature. As we can see, the phase curvature obtained with the FCT is a continuous line as expected. On the other hand, we can see that the phase curvature obtained with the RPT technique is a line with one abrupt change, therefore, the phase obtained $\hat{\phi}$ with the RPT is $\hat{\phi} \notin C^2$ while the FCT obtains a phase $\hat{\phi} \in C^2$. Both phase profiles in Fig. 2.3(b) and 2.3(c) are compatible with the one-dimensional fringe pattern signal given in Fig. 2.3(a). However, estimated phase profile $\hat{\phi} \in C^2$ shown in Fig. 2.3(b) is typical phase profile of a fringe pattern with closed fringes. As our final intention is to demodulate SFPI with closed fringes, we restrict phase solutions to those phase profiles which are $\hat{\phi} \in C^2$.

Summing up, until here we have developed a demodulation method with a frequency estimator (Eq. 2.22) that searches in a discrete frequency set. It was tested for one-dimensional signals without carrier as is shown in Fig. 2.3. Now, we are going to apply the method in two-dimensional signals.

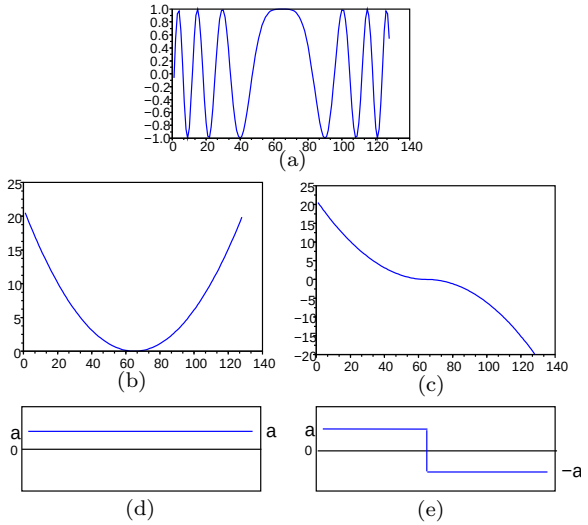

Fig. 2.3: In graph 1) a signal is shown which phase is modeled as $\phi(x) = \frac{1}{2}ax^2$. In graph 2) we show the obtained phase using the FCT and in graph 4) we show its curvature. In graph 3) we show the obtained phase using the RPT technique and in 5) we show its curvature. As we can see, the phase curvature presented in 4) is a continuous line while the phase curvature in 5) has one abrupt variation.

2.3 Two-dimensional case

In this case we are going to implement the frequency curvature tracker or FCT method, to demodulate square frames into the image interferogram lattice around a given site as a starting seed. To do this, we are going to use the FCT (see subsection 2.2.1) using a row by row scanning strategy to demodulate sequentially all sites in the frame. Each row and column is going to be treated as a one-dimensional signal.

Let (η, ξ) be the initial seed in the frame, where η is the column number and ξ is the row number. Then we set the phase of the initial seed as $\hat{\phi}(\eta, \xi) = \arccos[I'(\eta, \xi)]$, where $I'(\cdot)$ is defined as in Eq. (2.2). For a graph illustration see Fig. 2.4(Step 1), where the initial seed is shown. The next step is to demodulate the column of the initial seed using the FCT described in subsection 2.2.1, taking the column as a one dimensional signal as shown in Fig. 2.4(Step 2); the same is done for the row of the initial seed as shown in Fig. 2.4(Step 3). Finally, we scan row by row and each row is demodulated with the FCT, using as an initial seed the value of the column as shown in Fig. 2.4(Step 4). Thus, we have a row by row demodulation process to demodulate a square frame in a image interferogram.

Our strategy to demodulate an image interferogram following an arbitrary path is by following the path with square frames as is shown in Fig. 2.5. Therefore, we explained before how to demodulate a frame. As we can see in Fig. 2.5, a frame in a site slope the frame of the neighbor site. Then, to maintain a spatial coherence between frames, only the seed of the first demodulated frame is set using the arc cosine function. The seed of the subsequent frame is already estimated in the previous frame.

2.4 Tests and results

Now let us to test FCT method with a simulated SFPI with closed fringes following an arbitrary path. We are going to compare this result with the result of RPT method following an arbitrary path. For this, we propose a free hand drawn path. In Fig. 3.2(a) we see the

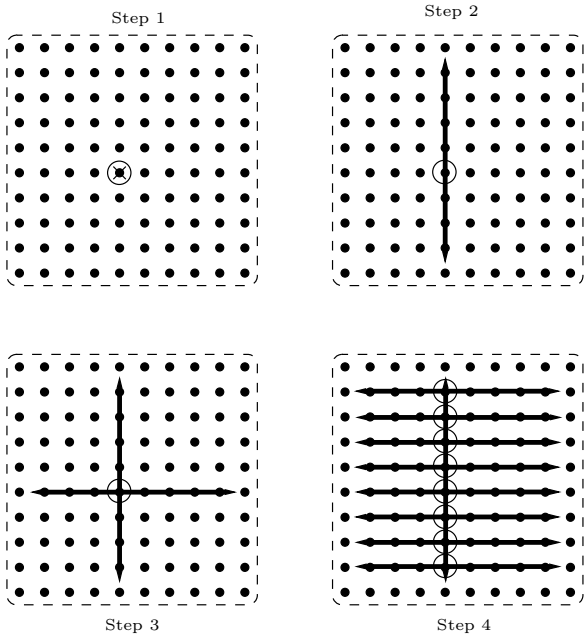

Fig. 2.4: Steps for the row by row scanning strategy to demodulate a frame in the image interferogram lattice. *Step 1* shows the initial seed with a circle, *Steep 2* shows the column demodulation, *Step 3* shows the row demodulation and *Step 4* the row by row scanning to demodulate each row using the values of the column as an initial seed for each row.

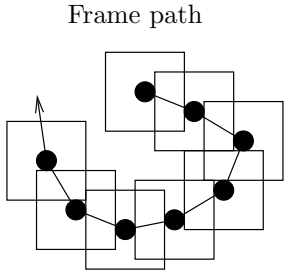

Fig. 2.5: In this figure we illustrate a path that is followed with square frames. Each site of the path, represted with a dark point, is the center of its frame and each frame is such that intersects the frame of the neighbor site and the neighbor site belong to this intersection.

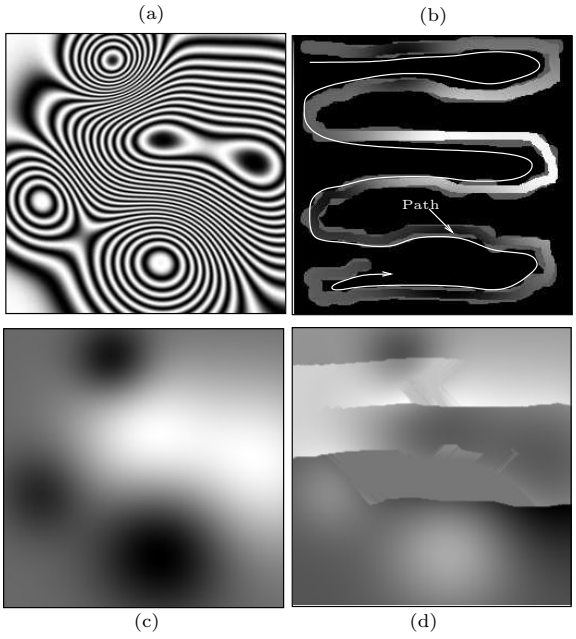

Fig. 2.6: (a) is the simulated image interferogram $I'(x, y)$, (b) is the path to follow, (c) is the demodulated phase using the FCT in two dimensions and (d) is the demodulated phase using the RPT.

generated SFPI $I'(x, y)$ while in Fig. 3.2(b) the drawn path to follow. We can see the phase obtained using the FCT in Fig. 3.2(c) while in Fig. 3.2(d) the phase obtained with the RPT following the proposed path. As we can see, the RPT fails to obtain the expected modulated phase. On the other hand, we can see that the FCT obtains the expected modulated phase even if we are not following the fringes. In this sense, the FCT is more robust than the RPT since it obtains the expected phase without taking care on following fringes.

Figure 2.7, shows two even more complicated fringe structures to demonstrate the FCT method's ability to demodulate complicated fringes without following the fringes. The actual phase of the fringe patterns shown in Figs. 2.7(a) and 2.7(b), were generated using a linear combination of Gaussian functions.

Figure 2.8, shows an experimental SFPI generated with ESPI technique for contouring.

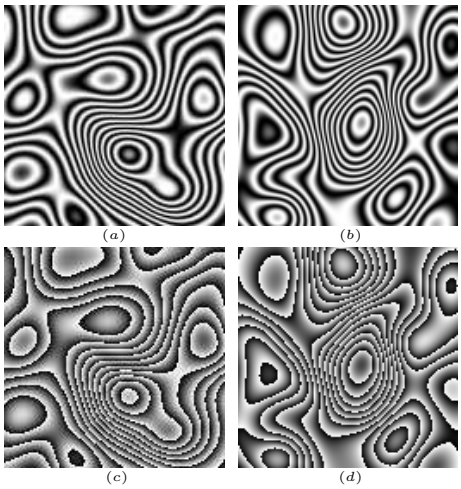

Fig. 2.7: A more complicated structure of fringes. (a) and (b) are simulated fringe patterns and (c) and (d) shows its estimated phase with the FCT using a row by row scanning strategy. The phase is shown wrapped for illustration purposes.

As the FCT method assume that the modulating phase of the SFPI is continuous in curvature, we can not apply directly the FCT method to the image interferogram shown in Fig. 2.8(a). Firstly, we must use a normalization method able to normalize and filter the fringe pattern. In this case we have used the normalization method reported in Ref. Guerrero et al. [2005] tuning properly the filters. Figure 2.8(b) shows the obtained normalized fringe pattern. The estimated phase is shown in Fig. 2.8(c) while Fig. 2.8(d) shows the estimated phase wrapped for illustration purposes.

2.4.1 Computational time cost report

We have tested the FCT method for various interferogram sizes and demodulated successfully. The computational time cost for the different interferogram image sizes is as follow: size of 1024×1024, 1.14 seconds; size of 512×512, 0.320 seconds; size of 256×256, 0.089 seconds; size of 128×128, 0.016 seconds. These tests were made on a personal computer with a 64bit processor at 2GHz and 1GB of memory RAM using double precision data.

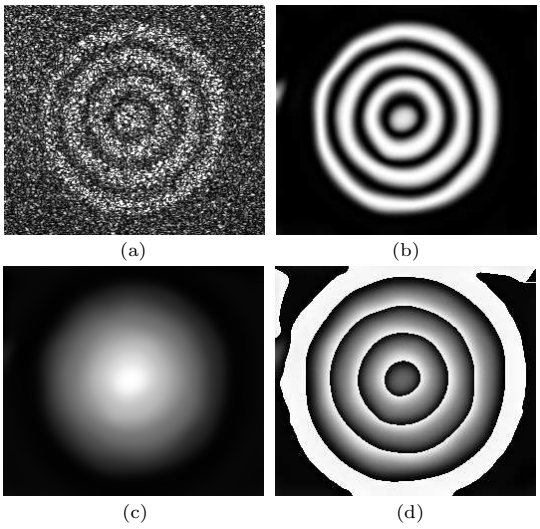

Fig. 2.8: (a) is a real experimental SFPI, (b) is its normalized version, (c) is the obtained phase with the FCT using a row by row scanning strategy and (d) is the wrapped phase showed for illustration purposes.

The FCT algorithm was programmed using a "C" compiler.

2.5 Discussion and Conclusions

Here, we have demonstrated that estimating the phase into a function space C^2, removes the local ambiguities given by the actual phase estimators as the RPT (see Fig. 2.2). To estimate the phase into the function space C^2, we have developed an estimator based on the local frequency estimation within a discrete frequency set. The main advantage of this estimator is that we can to demodulate a SFPI with closed fringes regardless of the path to follow (see Fig. 3.2). Another advantage is that we do not need to use a minimization process like the *steepest-descent* algorithm (see Ref. **?**) for non linear systems to estimate the phase as the RPT method. As we can see in subsection 2.4.1, this method is a fast demodulation process. Finally, we can use a simple row by row scanning strategy like the one shown in Fig. 2.4 to demodulate the image interferogram. This is important because

we do not need program complicated fringe following algorithms.

On the other hand, proposed method assumes that the modulating phase is continuous and that fringe pattern is normalized. Then, we can not apply this method directly to an image interferogram like that shown in Fig. 2.8. It is necessary to preprocess the SFPI to normalize and filter the fringes. This is a drawback of the FCT method as is, because it can not be applied to a noise contaminated experimental fringe pattern directly. However, this drawback does not diminish the importance of the suggested method and its ideas (estimating the phase $\hat{\phi}$ as $\hat{\phi} \in C^2$). This is because phase profiles which are in C^2, are typical phase profiles of single fringe pattern images with closed fringes. Furthermore, nowadays there is not one published work with a path independent technique to demodulate single image interferograms with closed fringes. At present, we are working with some ideas to apply these concepts within a modified robust FCT method to be applied directly to noise contaminated fringe patterns.

It should be clearly remarked, that as shown by the results of Figs. 3.2, 2.7 and 2.8, the method obtains the expected phase regardless of the path followed by the FCT. If the underlying modulating phase is continuous and at least one time differentiable, then the method is guaranteed to be path independent and able to recover the phase.

Chapter 3

Local Adaptable Quadrature Filters for Interferograms with closed fringes

Here, we propose a new approach to demodulate a single fringe pattern with closed fringes by using Local Adaptable Quadrature Filters (LAQF). Quadrature filters have been widely used to demodulate complete image interferograms with carrier frequency. However, in this paper, we propose the use of quadrature filters locally, assuming that the phase is locally quasimonochromatic, since quadrature filters are not capable to demodulate image interferograms with closed fringes. The idea, in this paper, is to demodulate the fringe pattern with closed fringes sequentially, using a fringe following scanning strategy. In particular we use linear *robust quadrature filters* to obtain a fast and robust demodulation method for single fringe pattern images with closed fringes. The proposed LAQF method does not require a previous fringe pattern normalization. Some tests with experimental interferograms are shown to see the performance of the method along with comparisons to its closest competitor, which is the Regularized Phase Tracker (RPT), and we will see that this method is tolerant to higher levels of noise [Estrada et al., 2007].

3.1 Introduction

In *moiré* interferometry, as well as in other areas of optical metrology, when one is working with transient events, one can have situations where it is necessary to deal with a single fringe pattern with closed fringes. As the information of interest is phase modulated by the fringe pattern, it is necessary to apply a demodulation method able to demodulate a single fringe pattern with closed fringes.

A single fringe pattern with closed fringes is typically modeled in the following way:

$$I(x, y) = a(x, y) + b(x, y)\cos[\phi(x, y)], \tag{3.1}$$

where $a(x, y)$ is the background illumination and $b(x, y)$ the modulation term or contrast. The phase to be demodulated is $\phi(x, y)$. If the fringe pattern has a carrier frequency, then it can be modeled in the following way:

$$I(x, y) = a(x, y) + b(x, y)\cos[\phi(x, y) + \omega x], \tag{3.2}$$

where $\phi(x, y)$ is the modulating phase, and ω is the carrier frequency. In this case, we can demodulate the fringe pattern by using quadrature filters like those used with the Fourier transform method Takeda et al. [1982], and the Hilbert transform method Kreis [1986]. In both cases, we obtain the wrapped modulating phase $\phi(x, y)$. However, this kind of methods fails to obtain the modulating phase when we have a fringe pattern like the one shown in (3.1), or in other words, when we have a single fringe pattern with closed fringes.

In this paper we are going to show a new approach to demodulate single fringe pattern images with closed fringes, using Local Adaptable Quadrature Filters (**LAQF**). In general, a quadrature filter is a band-pass filter that is zero in one half of the Fourier domain, and maps its input to a complex space. For example, if the input is a fringe pattern like the one shown in Eq. (3.1), the output is a complex signal whose real part is the fringe pattern itself, and the imaginary part is its quadrature. However, when we have closed fringes, the input signal quadrature, obtained with a quadrature filter, has abrupt sign changes when

applied to the complete fringe pattern Kreis [1986]. Hence, quadrature operators have been proposed to overcome this drawback, i.e. the Larkin's quadrature operator and the n-dimensional quadrature transform Larkin et al. [2001], Larkin [2001], Servin et al. [2003].

Since a quadrature filter is not able to recover the expected phase from a complete single fringe pattern with closed fringes, we propose the use of adaptable quadrature filters in small regions where the phase may be considered quasimonochromatic. One of the advantages of using quadrature filters, is that we need only a band-pass filtering to remove the background illumination from the image interferogram. Then we use the LAQF to estimate the phase sequentially using a fringe following scanning strategy. This sequential way, used to demodulate a single fringe pattern with closed fringes, remind us of the first proposed sequential method, called the Regularized Phase Tracker (**RPT**) Servin et al. [2001], with the difference that we use local quadrature filters to estimate the phase.

As we are going to compare the LAQF method, developed here, with the RPT method shown in Servin et al. [2001], let us to show, in brief, the use of the RPT method to demodulate single fringe pattern images with closed fringes. Also, we are going to comment the derived RPT methods that have been published recently.

3.1.1 RPT method

To demodulate the phase, using the RPT method, we minimize the following functional with respect to $\hat{\phi}(x,y)$ and frequencies $u(x,y)$ and $v(x,y)$:

$$U[\hat{\phi}(x,y),u(x,y),v(x,y)] = \sum_{(\eta,\xi)\in\Gamma} \left\{ [\cos p(\eta,\xi) - I'(\eta,\xi)]^2 + \lambda[\hat{\phi}(\eta,\xi) - p(\eta,\xi)]^2 \right\}, \quad (3.3)$$

where $p(\eta,\xi) = \hat{\phi}(x,y) + u(x,y)(x-\eta) + v(x,y)(y-\xi)$ is a phase plane and $\hat{\phi}(x,y)$ is the estimated phase at site (x,y) after the minimization. The closed region Γ is a neighborhood around site (x,y), and λ is a regularization parameter to strengthen the method against noise. $I'(x,y)$ is the fringe pattern shown in Eq. (3.1), but normalized in the following way:

$$I'(x,y) = \cos[\phi(x,y)] \quad (3.4)$$

where background illumination $a(x, y)$ is removed using a high-pass filter, and the modulation term $b(x, y)$ is spatially normalized to the constant value 1, using normalization techniques for fringe patterns Quiroga et al. [2001], Quiroga and Servin [2003], Guerrero et al. [2005]. Then, the RPT method needs a previous fringe pattern normalization to remove the contrast variations of the image interferogram.

To obtain the expected phase using the RPT, it is necessary to use a scanning strategy to follow the fringes. This scanning strategy first visits the sites from the fringe pattern that are in the same isophase contour, i.e. following the fringes. One can find an algorithm with this feature for the scanning strategy in Ref. Strobel [1996]. As our approach also needs this scanning strategy to obtain the expected phase, we will refer to this scanning strategy as the Fringe Following Scanning (**FFS**) throughout this paper.

Then, to demodulate an experimental interferogram with closed fringes, using the RPT, we do the following main steps in the demodulation process:

1. Apply a band-pass filter to remove the background illumination and attenuate the noise.

2. Normalize the fringe pattern in order to make the contrast component, $b(x, y)$, spatially constant.

3. Demodulate the fringe pattern using the RPT.

In step 1, band-pass filtering may be easily achieved using low-pass filtering followed by high-pass filtering. For example, the following spatial filter may be used to apply a band-pass filter:

$$g_\sigma(x, y) = \exp\left[\frac{-(x^2 + y^2)}{\sigma^2}\right], \tag{3.5}$$

where σ controls the filter band-width. Having this, we can apply a band-pass filter in the following way:

$$I'(x, y) = [I - I * g_{\sigma_H}(x, y)] * g_{\sigma_L}(x, y), \tag{3.6}$$

where $*$ is the convolution operator, $I(x,y)$ is the image insterferogram modeled in (3.1), and $\sigma_L \ll \sigma_H$, i.e, $\sigma_L = 2.4$ and $\sigma_H = 80$, for 256×256 image interferograms or bigers. This process can be implemented in a fast way by using the fast Fourier transform Brigham [1974].

Step 2 is more complicated, since it is necessary to obtain a pre-estimated phase map to normalize the fringe pattern (see Quiroga et al. [2001], Quiroga and Servin [2003], Guerrero et al. [2005]), i.e, the simplest way to normalize a single fringe pattern with closed fringes may be using the Fourier transform method reported in Takeda et al. [1982], however, this technique may introduce undesired artifacts in the fringe pattern. For this reason, to estimate the phase of experimental interferograms, the RPT method spends most of the computational time in the normalization rather than in the demodulation process itself.

Other known approaches to demodulate single fringe patterns with closed fringes that need a previous fringe pattern normalization are the Larkin's quadrature operator Larkin et al. [2001], Larkin [2001], and the n-dimensional quadrature transform Servin et al. [2003]. These methods need a normalized fringe pattern to estimate the fringe orientation angle.

As the fringe pattern normalization may on occasions turn out to be as difficult as obtaining the phase, in Ref. Legarda-Sáenz et al. [2002] another version of the RPT method was proposed to deal with the modulation term. Then, the modified RPT functional, proposed in Legarda-Sáenz et al. [2002], may be written as the following:

$$\begin{aligned} U[\hat{\phi}, u, v, \hat{b}, b_x, b_y] &= \sum_{(\eta,\xi)\in\Gamma} \Big\{ [\beta(\eta,\xi)\cos p(\eta,\xi) - I'(\eta,\xi)]^2 \\ &+ \lambda[\hat{\phi}(\eta,\xi) - p(\eta,\xi)]^2 \\ &+ \mu[\hat{b}(\eta,\xi) - \beta(\eta,\xi)]^2 \Big\}, \end{aligned} \tag{3.7}$$

where $\hat{b}$ is the modulation estimation, and b_x and b_y its partial derivatives in x and y respectively. We have removed the (x,y) dependence of each variable for more clarity. The term $\beta(\eta,\xi)$ is a modulation plane defined as $\beta(\eta,\xi) = \hat{b}(x,y) + b_x(x,y)(x-\eta) + b_y(x,y)(y-\xi)$. If we see Eq. (3.3) and Eq. (3.7), we can see that the modified RPT method reported in

Legarda-Sáenz et al. [2002], estimates the phase and frequencies along with the modulation term and its derivatives. As a consequence, using the modified RPT method reported in Legarda-Sáenz et al. [2002], let us solve a non-linear system with more time-consuming numerical methods, than the numerical methods used to solve the non-linear system of the original RPT reported in Servin et al. [2001].

More recently, in Ref. Rivera [2005], a half-quadratic linearized RPT functional was proposed for the phase estimation that let us solve a linear system instead of the original RPT non-linear system. Taking this idea, and the idea shown in Legarda-Sáenz et al. [2002] to estimate the phase and modulation term, in Ref. Legarda-Saenz and Rivera [2006] a linearized modified RPT method is presented to estimate the phase and modulation term by solving a linear system. The main advantage in this work is that one can have a linearized RPT method that estimates the phase and modulation term in the same process as using Eq. (3.7), but much faster (see Legarda-Saenz and Rivera [2006]).

All versions of the RPT method, mentioned in the last paragraph, model the phase estimation and the modulation or contrast component of the image interferogram, by using a cost functional like the shown in Eq. (3.7). As a result, these modified RPT methods are more robust than the original RPT that uses Eq. (3.3), when the image interferogram is not normalized. However, if we see Eq. (3.3) and Eq. (3.7), these RPT like methods support the same levels of noise than the original RPT, since the added terms in Eq. (3.7) just deal with the modulation variations.

In this paper we present the local adaptable quadrature filter method or LAQF method, which does not need a previous fringe pattern normalization like the modified RPT methods shown in Legarda-Sáenz et al. [2002], Rivera [2005], Legarda-Saenz and Rivera [2006], and let us solve a linear system like the method reported in Legarda-Saenz and Rivera [2006]. As we use local quadrature filters to estimate the local phase, rather than estimate the local phase by fitting a phase plane with the RPT method, the LAQF method reported here supports higher levels of noise than the RPT like methods.

In section 3.2 we are going to show in detail the LAQF method, which particularly uses Robust Quadrature Filters Marroquin et al. [1997] to estimate the phase locally. In section 3.3, we are going to present comparisons between the proposed method and the RPT to see that this method, with a simple band-pass filtering, is able to demodulate noisier fringe patterns than the RPT method. Also, we will show some experimental interferograms to see its performance with real fringes. Finally, in section 3.4 we will talk about the conclusions of the work.

3.2 Proposed LAQF method

As we said before, in this method we only use a band-pass filtering previous to the fringe pattern demodulation using the LAQF. Then, here it is not necessary to normalize the fringe pattern.

Assuming that we apply a band-pass filtering to the fringe pattern given in (3.1), we obtain the following fringe pattern:

$$I(x, y) = b(x, y) \cos[\phi(x, y)], \tag{3.8}$$

where (x, y) is a site in L, being L the lattice where the interferogram is recorded. Now, assume that in a small region Γ around site (x, y), the fringe pattern locally is quasi-monochromatic. Then, locally the fringe pattern looks like:

$$I_0(\eta, \xi) = b(\eta, \xi) \cos[\phi(x, y) + u_0(x - \eta) + v_0(y - \xi)], \tag{3.9}$$

where $(\eta, \xi) \in \Gamma$ and (u_0, v_0) are the local frequencies in x and y respectively. As one can see in Eq. (3.3), the RPT method also uses this assumption and fits the observed data in Γ around (x, y) with a phase plane to estimate the phase at site (x, y) (see Eq. 3.3). Although this technique works properly, we have found a better and more robust way using local adaptable quadrature filters to estimate the phase sequentially.

In particular, to estimate the phase in region Γ around site (x, y), we use the Robust Quadrature Filters developed in Marroquin et al. [1997], to locally demodulate the fringe pattern. However, we do not apply these filters to the complete image interferogram as are presented in Marroquin et al. [1997], but we apply these filters locally in a small region Γ around a site (x, y), and we adapt its tuning frequency as we move through the image interferogram's sites using a fringe following scanning or FFS. Hence, we call this method local adaptable quadrature filters or LAQF along this paper.

Then, the LAQF uses robust quadrature filters to locally estimate the phase. This process is done by minimizing the following cost functional in region Γ around site (x, y):

$$U[f] = R_\Gamma[f, I] + \lambda V_\Gamma[f], \tag{3.10}$$

where the filter estimation model f is complex and can be expressed as $f(\eta, \xi) = \varphi(\eta, \xi) + i\psi(\eta, \xi)$, for $(\eta, \xi) \in \Gamma$.

The first term $R_\Gamma[f, I]$ in (3.10) is commonly known as the data term, and it depends on the difference between the observed data I (in this case the interferogram) and the estimation model f, in such a way that $R_\Gamma[f, I]$ is minimal when f is close to I. Here, we define $R_\Gamma[f, I]$ as the residual between the finite differences of the observed data and the finite differences of the filter estimation model in the following way:

$$R_\Gamma[f, I] = \sum_{(\eta,\xi)\in\Gamma} \|f_x(\eta, \xi) - 2I_x(\eta, \xi)\|^2 + \|f_y(\eta, \xi) - 2I_y(\eta, \xi)\|^2, \tag{3.11}$$

where f_x and I_x, are the finite differences in x and f_y, and I_y are the finite differences in y. For example, the finite differences for f in x may be given as $f_x(x, y) = f(x, y) - f(x-1, y)$, and so on. We define the data term in this way because if we take its Fourier transform, this term has a zero in the origin, which is a desired feature in the use of quadrature filters to demodulate fringe patterns (see Kreis [1986]).

The second term $V_\Gamma[f]$ is usually called the regularization term. This term adds restrictions to the estimation model f. For example, a commonly used regularization term to

restrict the filter estimation model f from being smooth (to obtain a low-pass filter), is the quadratic norm of the *Laplacian*'s operator known as the *membrane model*. In our case, since we want a quadrature filter, we define the regularization term in the following way, according to Ref. Marroquin et al. [1997]:

$$V_\Gamma(f) = \sum_{(\eta,\xi)\in\Gamma} \left\{ \|f(\eta,\xi) - f(\eta-1,\xi)e^{-iu_0}\|^2 + \|f(\eta,\xi) - f(\eta,\xi-1)e^{-iv_0}\|^2 \right\}, \qquad (3.12)$$

where $i = \sqrt{-1}$, u_0 is the tuning frequency in x, and v_0 the tuning frequency in y. In the Fourier domain, this term, along with $R_\Gamma[f, I]$, looks like a band-pass filter that is zero in one half of the Fourier domain, and maximum in frequency (u_0, v_0) (see Marroquin et al. [1997]). The parameter λ in (3.10) is known as the regularization parameter that controls the strength of the quadrature filter (or its bandwidth).

To minimize Eq. (3.10), we obtain its gradient with respect to f and equal it to zero. Then, we can solve the resulting linear equation system using fast straightforward algorithms such as the *Gauss-Seidel* algorithm, although we can use more generic algorithms, like the *Steepest-descent* used by the RPT method **?**Servin et al. [2001]. In Ref. Marroquin et al. [1997], the gradient of cost functional (3.10) is given explicitly.

Thus, to obtain the local phase in region Γ around site (x, y), we minimize Eq. (3.10) with respect to f using the tuning frequency (u_0, v_0). Once given the quadrature filter f by minimizing (3.10), we obtain the phase (modulus 2π) in region Γ as:

$$\hat{\phi}(\eta,\xi) = \arctan\left[\frac{\psi(\eta,\xi)}{\varphi(\eta,\xi)}\right]. \qquad (3.13)$$

Given the phase in region Γ around the current site (x, y) by using (3.13), we move to the next site using the fringe following scanning or FFS as with the RPT. Just before we move to the next site, however, we need to update the LAQF tuning frequency to estimate the phase correctly in region Γ around the next site. The local frequencies for current site (x, y) may be used as the tuning frequency to estimate the phase in the next site, and are obtained as the finite differences along x and y of the estimated phase given by (3.13). But,

as we see from Eq. (3.13), the estimated phase in region Γ around site (x, y) is wrapped into the $[-\pi, \pi]$ interval. For this reason, we take the local frequencies for the current site (x, y) in the following way:

$$u_0 = \arctan\left[\frac{\sin[(\hat{\phi}(x,y) - \hat{\phi}(x_+,y))(x - x_+)]}{\cos[(\hat{\phi}(x,y) - \hat{\phi}(x_+,y))(x - x_+)]}\right] \tag{3.14}$$

and

$$v_0 = \arctan\left[\frac{\sin[(\hat{\phi}(x,y) - \hat{\phi}(x,y_+))(y - y_+)]}{\cos[(\hat{\phi}(x,y) - \hat{\phi}(x,y_+))(y - y_+)]}\right], \tag{3.15}$$

where x_+ and y_+ are the coordinates of the previous already phase estimated site, given by the FFS, and they may take the following values:

$$x_+ = \begin{cases} x+1 & \text{If previous site is to the right} \\ x-1 & \text{If previous site is to the left} \end{cases} \tag{3.16}$$

and

$$y_+ = \begin{cases} y+1 & \text{If previous site is down} \\ y-1 & \text{If previous site is up} \end{cases}, \tag{3.17}$$

For illustration purposes, In Fig. 3.2, we see an example of the estimated phase in the region Γ of size 32×32 around site $(32, 32)$ from the given fringe pattern. Here, we used the tuning frequency $(u_0, v_0) = (0.25, 0.24)$ with $\lambda = 50$ to obtain the phase in Γ. We must remark that in this case, for illustration purposes we have chosen a region size too big compared with the sizes of $n \times n$, with typically, $n \in 5, 6, 7, 8$.

The scanning strategy to demodulate all sites from the fringe pattern with the LAQF is the same FFS used by the RPT method, as we said before. We start at site (x, y) as the initial seed to demodulate the fringe pattern. Then, we visit each site from the fringe pattern using the FFS. For each visited site, we estimate its local phase by minimizing Eq. (3.10) and using Eq. (3.13). After this, we obtain the tuning frequency for the next site to visit using (3.14) and (3.15).

To estimate the phase for the initial seed (x, y), we must know previously the tuning frequency to use. Here, we propose a simple way to choose the initial seed (x, y) and its

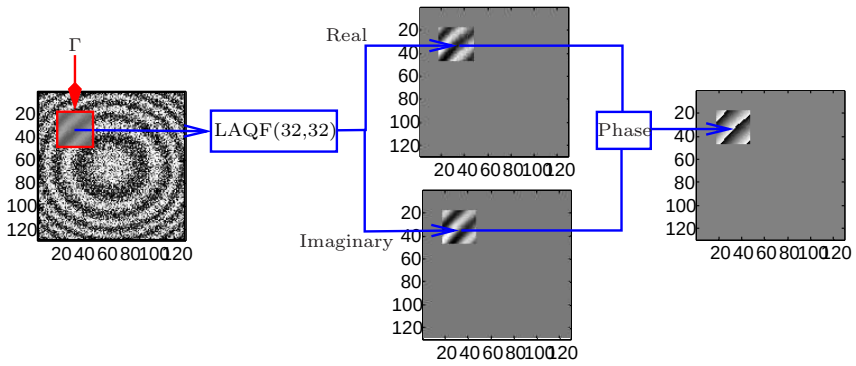

Fig. 3.1: In this figure, we graphically illustrate how the phase in region Γ around site $(32, 32)$ is obtained. The left image is the given interferogram where we mark the neighborhood in red. The intermediate images are the real part and imaginary part of the local quadrature filter, or LAQF, obtained after minimizing Eq. (3.10). Finally, the right image is the local phase obtained from the RQF.

tuning frequency by using a Gabor filter. A Gabor filter is a quadrature filter defined in the following way:

$$g_{u_0,v_0}(x,y) = \exp\left[\frac{-(x^2+y^2)}{\sigma^2}\right] e^{-i(u_0 x + v_0 y)}, \tag{3.18}$$

where σ controls the bandwith of the Gabor filter, and (u_0, v_0) are its tuning frequencies. Thus, we tune the Gabor filter onto a frequency (u_0, v_0) that can be in the fringe pattern. Then, we filter the fringe pattern with the tuned Gabor filter. Finally, we take as initial seed the site (x, y) for which the Gabor filter magnitude response is maximal. For example, suppose that $\tilde{I}$ is the filtered fringe pattern with the Gabor filter tuned to the frequency (u_0, v_0), then we take as initial seed the site:

$$(x,y) = \arg\max_{(x_i,y_i)} \|\tilde{I}(x_i,y_i)\|, \tag{3.19}$$

then we use the tuning frequency (u_0, v_0) to start the demodulation process.

Readers may wonder why use a Gabor filter to choose the initial seed and its tuning frequency instead of the robust quadrature filter shown in Eq. (3.10). The answer is because

in this case, we apply the Gabor filter to the complete fringe pattern, which is faster than minimizing (3.10) for the complete pattern. Another question could be why not to use just Gabor filters instead of the robust quadrature filters to filter the local region Γ in the demodulation process. The answer is that since the Gabor filters are convolution filters, they introduce errors on the edges of the region where the filter is applied. As the region's sizes used here are small, to ensure the validity of the assumption of local quasimonochromatic phase, errors introduced on the edges by using convolution filters are significant in these small regions. Hence, we use the robust quadrature filters locally, because these filters have no problems on the region's edges.

3.3 Tests and results

In all tests presented here, we demodulate the given single fringe patterns with closed fringes successfully, using the following basic steps:

1. Apply a band-pass filter to attenuate the noise and remove the background contribution.

2. Demodulate the fringe pattern using the LAQF as described in previous section.

To apply the band-pass filter, we used Eq. (3.6) with $\sigma_L = 2.5$ and $\sigma_H = 80$ using a fast Fourier transform algorithm Brigham [1974]. The computational time spent in this process, for a 256×256 image insterferogram, was of 0.543 seconds. For our tests we used a 64bit personal computer architecture in a Linux like operating system, and a C-language 64bit optimized compiler.

In our first test, we show the levels of noise that the LAQF tolerates, and compare our results to those obtained with the RPT method. In Fig. 3.2, we see a table with the obtained results. The fringe patterns shown there were computer generated with the ground truth phase shown in Fig. 3.3, adding a phase noise whose probability distribution

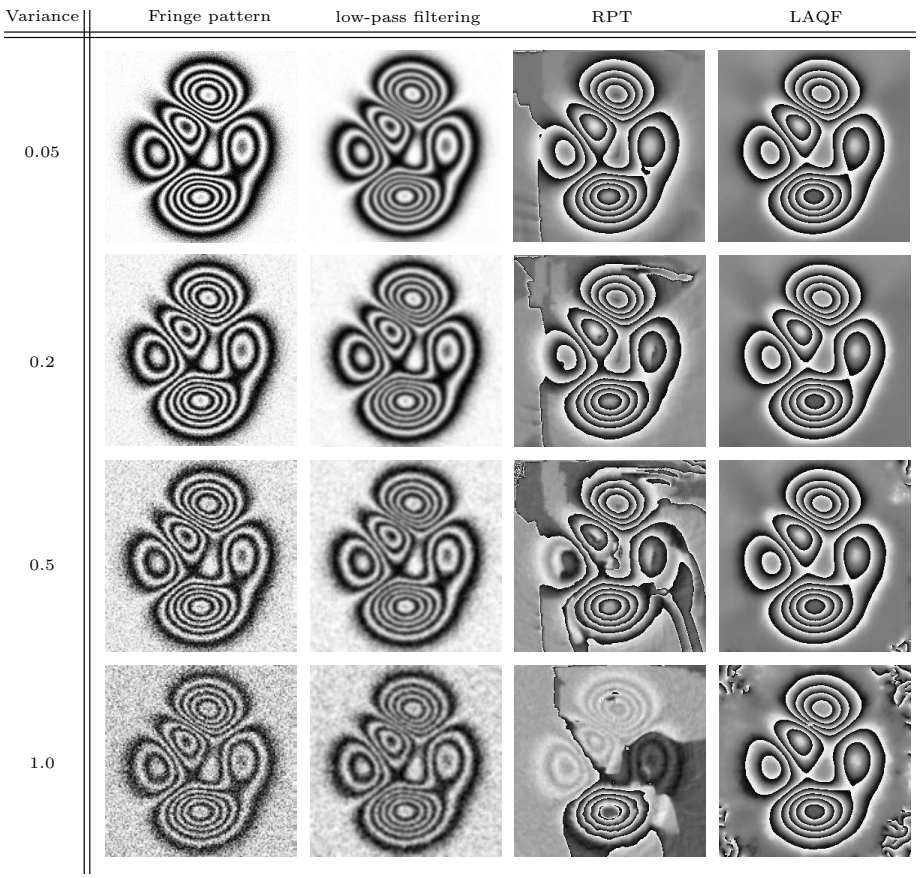

Fig. 3.2: In this figure: the variance column shows the variance of the Gaussian noise added to the ground truth phase; the fringe pattern column shows the generated fringe pattern; the RPT column shows the obtained phase using the RPT method and the LAQF column the phase obtained using the LAQF.

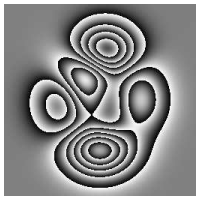

Fig. 3.3: Ground truth phase used to generate the fringe patterns shown in Fig. 3.2.

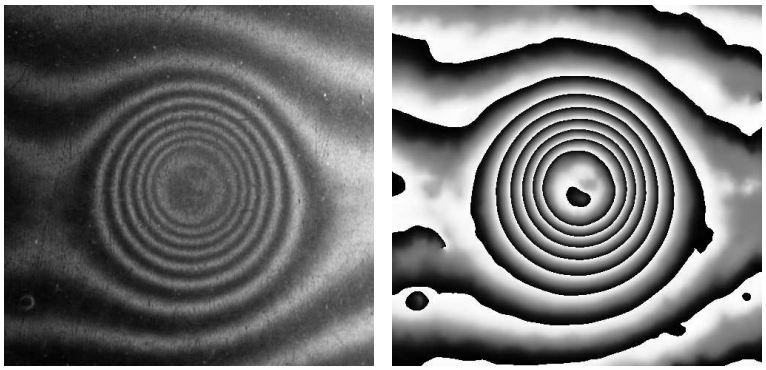

(a) (b)

Fig. 3.4: (a) image interferogram with closed fringes obtained by means of a moiré technique. (b) expected obtained phase using LAQF. The image interferogram dimensions are 488×500.

is Gaussian with mean zero and variance given in the variance column. Here, the fringe patterns are already normalized in order to be used with the RPT directly. The parameters used with the RPT method are $\lambda = 20$ and neighborhood size 6×6. The parameters used with the LAQF are $\lambda = 5$, neighborhood Γ size 6×6.

The computational cost time in these tests, where the fringe pattern's size is of 256×256, was 11.1 seconds for the RPT and 4.224 seconds for the LAQF.

As one can see in Fig. 3.2, the phase obtained in all cases with the LAQF method looks like the ground truth phase shown in Fig. 3.3, unlike the phase obtained with the RPT method, which differs from the ground truth phase as the noise grows.

In the second test, we show an experimental interferogram with closed fringes generated using a moiré technique to measure deformations on surfaces. In Fig. 3.4(a), we see the image interferogram, and in Fig. 3.4(b) its obtained phase with the LAQF. The parameters used in this test are $\lambda = 5$ and neighborhood Γ size 8×8.

The next experiment shows what happens when the image interferogram has very low frequency zones. In Fig. 3.5(a), we see an image interferogram with closed fringes generated with a moiré technique. This image interferogram has zones where its frequency is

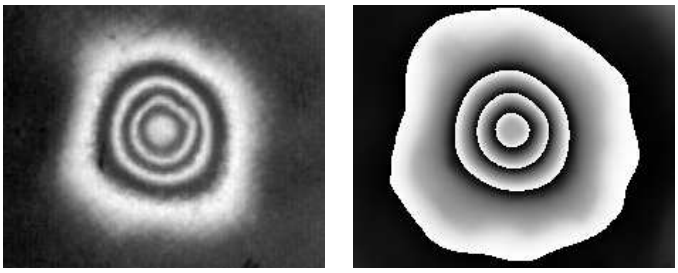

(a) (b)

Fig. 3.5: (a) image interferogram with very low frequency zones. The image interferogram was generated with a moiré technique. (b) phase obtained using the LAQF.

practically zero. In Fig. 3.5(b), we see the obtained phase using the LAQF. As we can see, the LAQF method behaves correctly in zones where the frequency is practically zero.

Finally In Fig. 3.6(a), we show another image interferogram. In this case, the fringes are available only in a zone of the image. To demodulate this kind of interferograms, a mask is used to indicate the zone where the fringes exist. As we can see, the phase is obtained correctly.

3.4 Discussion and conclusions

The LAQF method, developed here, is a robust demodulation method for the recovery of phase from single fringe patterns with closed fringes without the need of normalization. This method, compared to the RPT method, tolerates higher levels of noise. As the RPT method, this method is a sequential method that uses a scanning strategy following the fringes.

The way to choose the Γ neighborhood size used for the LAQF, is the same way used to choose the neighborhood size for the RPT. This is by testing different sizes. By testing different sizes, we found that neighborhood sizes of $n \times n$ for $n \in \{5, 6, 7, 8\}$ are situable to demodualte correctly an image interferogram with closed fringes. Actually there is no

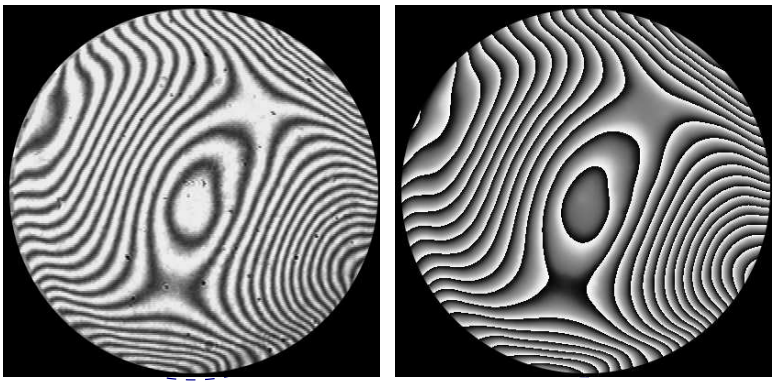

Fig. 3.6: (a) is the interferogram to demodulate, and (b) its demodulated phase using the LAQF. In this example, we see that the fringes exist just in a zone of the image.

rule to say what is the optimum neighborhood size to use, nither for the other secuential methods like the RPT.

The RPT method is a demodulation method that supports certain levels of noise. Other modified RPT methods that support variations in the modulation term from the fringe pattern, have been presented to demodulate single fringe patterns with closed fringes (see Rivera [2005], Legarda-Sáenz et al. [2002], Legarda-Saenz and Rivera [2006]). However, all these methods, as they are based on the RPT method, support the same levels of noise than the RPT. On the other hand, the LAQF approach estimates the modulating phase using local robust quadrature filters. The single common process between the RPT method and the LAQF method, presented here, is the fringe following scanning strategy used to demodulate the image interferogram.

Chapter 4

Future work and conclusions

In metrology, real-time analysis with traditional interferometer systems is almost impossible, because they need specular reflectors attached to especial mounts [Malacara et al., 1998]. The main problem here is the difficulty to introduce carrier frequencies in order to recover the phase as fast as needed. Hence, alternatives for real-time analysis such as holographic interferometry, or as some people call TV holography, are replacing the traditional interferometer systems because it is more relievable real-time analysis with holographic interferometry [Goodman, 2004]. For example, one can use pulsed digital holography for real-time analysis of mechanical stress or deformations [Pedrini et al., 1997]. However, to use this kind of techniques we need more powered and pulsed lasers because these systems use very small pupils to introduce the carriers needed and grab the holograms. In pulsed digital Holography are grabbed at least two holograms in the same image, after that, the information is recovered by using the Fourier transform, therefore, it is needed high resolution cameras as well. As a result, the money invested in digital holography is greather than the money invested for a simple Michelson interferometer, although we will not be able to do real-time analysis with a Michelson interferometer.

Actually, as the technology is advancing, every day is growing the necessity of optical systems for real-time analysis in metrology. This is because we have almost reached the future of measurement systems with the optical metrology. Taking this background, with the

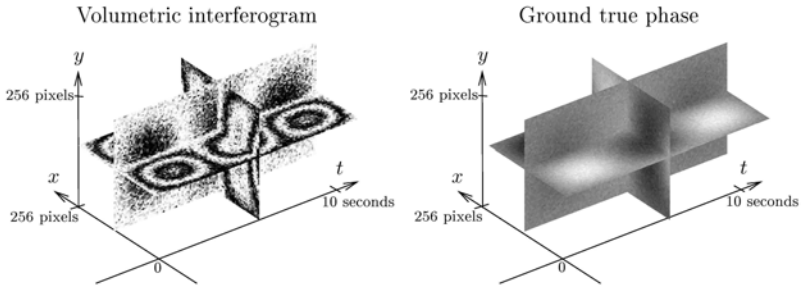

Fig. 4.1: A volumetric 3-dimensional interferogram without carrier frequencies in both space nor time. The left is the 3-dimensional interferogram and the right its ground true phase.

idea of simplify the interferometer systems, we bet, on the other hand, in the development of robust computer techniques to make real-time analysis in optical metrology, rather than in optical techniques to introduce frequency carriers.

In our days, there is no one robust demodulation technique for temporal interferograms without both spatial and temporal carriers. This is because the techniques developed until here, are designed for single image interferograms with closed fringes, that is, without spatial carrier [Servin et al., 1997, 2001, Larkin et al., 2001, Servin et al., 2003, 2004, Rivera, 2005, Villa et al., 2005, Estrada et al., 2006, 2007]. The problem to demodulate an interferogram sequence without both spatial and temporal carriers is the same as to demodulate a volumetric 3-dimensional interferogram like that shown in Fig. 4.1. In Fig. 4.1, we show an illustration of a volumetric 3-dimensional interferogram without carriers in any direction. The left shape is the 3-dimensional interferogram and the right its ground true phase.

One of the first complications to demodulate a volumetric interferogram like the shown in Fig. 4.1, using the techniques described by Servin et al. [1997, 2001], Larkin et al. [2001], Servin et al. [2003, 2004], Rivera [2005], Villa et al. [2005] and Estrada et al. [2007], is the necessity of following the fringes to recover the expected phase. If we translate these techniques into the three dimensional case, we must to implement a three dimensional fringe

follower algorithm which, as first lance, is very difficult since actually the interferogram sequence is given frame by frame and not as a volume like the shown in 4.1. Then, to demodulate an interferogram sequence we need a path independent demodulation techniche to throw the fringe follower implementation and simplify the process.

Here, in chapter 2, we have presented a path independent demodulation method for two-dimensional interferograms and could be easily translated to the three-dimensional case, though, this method has a very important drawback: is very sensitive to noise [Estrada et al., 2006]. To make more robust this method we need a more robust and fast frequency estimation method. In chapter 3 we have presented a lineal method to obtain the wrapped phase of an interferogram with closed fringes. We have shown that, if we obtain the phase following an smooth phase curvature, we have not to follow the fringes to obtain the expected phase. Then we can merge both methods to obtain a robust demodulation method with out need of following the fringes. This is very important because then we can extend the method to the 3-dimensional case of interferogram sequences. As the phase estimation is fast using local adaptable quadrature filters, in local regions, we can tray this method to make real-time analysis over time and use the strategies shown in chapter 2 to follow an smooth phase curvature. However, all of this needs to be proofed numerically.

Bibliography

Max Born and Emil Wolf. *Principles of Optics: Electromagnetic Theory of Propagation, Interference and Diffraction of Light*. Cambridge University Press, 7 edition, 1999.

E. O. Brigham. *The fast fourier tranform*. Prentice-Hall, 1974.

J. Bruning, D. R. Herriott, J. E. Gallagher, D. P. Rosenfel, A. D. White, and D. J. Brangaccio. Digital wavefront measuring interferometer for testing optical surface and lenses. *Appl. Opt.*, 13:2693–2703, 1974.

J. N. Butters and J. A. Leendertz. A double exposure technique for speckle pattern interferometry. *J. Phys. E: Sci. Instrum.*, (4):277–279, 1971.

J. C. Estrada, M. Servín, J. A. Quiroga, and J. L. Marroquín. Path independent demodulation method for single image interferograms with closed fringes within the function space C^2. *Optics Express*, 14:9687–9698, October 2006.

J. C. Estrada, M. Servín, , and J. L. Marroquín. Local adaptable quadrature filters to demodulate single fringe patterns with closed fringes. *Optics Express*, 15:2288–2298, January 2007.

Munther A. Gdeisat, David R. Burton, and Michael J. Lalor. Real-Time Fringe Pattern Demodulation with a Second-Order Digital Phase-Locked Loop. *Appl. Opt.*, 39(29):5326–5336, 10 October 2000.

Joseph W. Goodman. *Introduction to Fourier Optics*. Roberts & Company, 10 December 2004.

J. E. Greivenkamp. Generalized data reduction for heterodine interferometry. *Opt. Eng.*, 23:350–352, 1984.

J. A. Guerrero, J. L. Marroquin, and M. Rivera. Adaptive monogenic filtering and normalization of ESPI fringe patterns. *Opt. Lett.*, 30:318–320, November 2005.

P. Hariharan, B. F. Areb, and T. Eyui. Digital phase-stepping interferometry: A simple error-compensating phase calculation algorithm. *Appl. Opt.*, 26:3899, 1987.

T. Kreis. Digital holographic interference-phase measurement using the Fourier-transform method. *J. Opt. Soc. Am. A*, 3(6):847–855, 1986.

K. Larkin. Uniform estimation of orientation using local and nonlocal 2-D energy operators. *Opt. Express*, 13(20):8097–8121, 3 October 2005.

K. G. Larkin. Natural demodulation of two-dimensional fringe patterns. II. Stationary phase analysis of the spiral phase quadrature transform. *J. Opt. Soc. Am. A*, 18(8):1871–1881, August 2001.

K. G. Larkin, D. J. Bone, and M. A. Oldfield. Natural demodulation of two-dimensional fringe patterns. I. general background of the spiral phase quadrature transform. *J. Opt. Soc. Am. A*, 18(8):1862–1870, 2001.

R. Legarda-Saenz and M. Rivera. Fast half-quadratic regularized phase tracking for non-normalized fringe patterns. *J. Opt. Soc. Am. A*, 23(11):2724–2731, November 2006.

R. Legarda-Sáenz, W. Osten, and W. Jüptner. Improvement of the Regularized Phase Tracking Technique for the Processing of Nonnormalized Fringe Patterns. *Appl. Opt.*, 41(26):5519–5526, 10 September 2002.

D. Malacara, M. Servin, and Z. Malacara. *Interferogram Analisys for Optical Testing.* Marcel Dekker, 1998. Chap. 1.

J. L. Marroquin. Local phase from local orientation by solution of a sequence of linear systems. *J. Opt. Soc. Am. A*, 15(6):1536–1544, June 1998.

J. L. Marroquin, J. E. Figueroa, and M. Servin. Robust quadrature filters. *J. Opt. Soc. Am. A*, 14(4):779–791, April 1997.

G. J. Morgan. Least squares estimation in phase-measurement interferometry. *Opt. Lett.*, 7:386–370, 1982.

A. Mujeeb, V. U. Nayar, and V. R. Ravindran. Electronic Speckle Pattern Interferometry techniques for non-destructive evaluation: a review. *INSIGHT*, 45(5):275–281, May 2006.

G. Pedrini, P. Fröning, and H. Fessler. Transient vibration measurements by using multi-pulses digital holography. *Optics and Laser Technology*, 29(8):505–511, 1997.

J. A. Quiroga and M. Servin. Isotropic n-dimensional fringe pattern normalization. *Opt. Commun.*, 224:221–227, September 2003.

J. A. Quiroga, J. A Gómez-Pedrero, and A. García-Botella. Algorithm for fringe pattern normalization. *Opt. Commun.*, 197:43–51, September 2001.

J. A. Quiroga, Manuel Servin, and Francisco Cuevas. Modulo 2 fringe orientation angle estimation by phase unwrapping with a regularized phase tracking algorithm. *J. Opt. Soc. Am. A*, 19(8):1524–1531, 8 August 2002.

M. Rivera. Robust phase demodulation of interferograms with open or closed fringes. *J. Opt. Soc. Am. A*, 22(6):1170–1175, 2005.

J. Schwider, R. Burow, K. E. Elssner, J. Grzanna, R. Spolaczyk, and K. Merkel. Digital wavefront interferometry: Some systematic error sources. *Appl. Opt.*, 22:3421–3432, 1983.

M. Servin, D. Malacara, and R. Rodriguez-Vera. Phase-locked-loop interferometry applied

to aspheric testing with a computer-stored compensator. *Appl. Opt.*, 33(13):2589–2595, 1 May 1994.

M. Servin, J. L. Marroquin, and F. J. Cuevas. Demodulation of a single interferogram by use of a two dimentional regularized phase-tracking technique. *Appl. Opt.*, 36(19), July 1997.

M. Servin, J. L. Marroquin, and F. J. Cuevas. Fringe-follower regularized phase tracker for demodulation of closed-fringe interferograms. *J. Opt. Soc. Am. A*, 18(3):689–695, mar 2001.

M. Servin, J. A. Quiroga, and J. L. Marroquin. General n-dimensional quadrature transform and its application to interferogram demodulation. *J. Opt. Soc. Am. A*, 20(5):925–934, May 2003.

M. Servin, J. L. Marroquin, and J. A. Quiroga. Regularized quadrature and phase tracking from a single closed-fringe interferogram. *J. Opt. Soc. Am. A*, 21(3):411–417, 4 March 2004.

K. A. Stetson and W. R. Brohinsky. Fringe-shifting technique for numerical analysis of time-average holograms of vibrating objects. *J. Opt. Soc. Am. A*, 5:1472, 1988.

B. Strobel. Processing of interferometric phase maps as complex-valued phasor images. *Appl. Opt.*, 35(13):2192–2198, 1 May 1996.

M. Takeda, H. Ina, and S. Kobayashi. Fourier transform methods of fringe-pattern analysis for computer-based topography and interferometry. *J. Opt. Soc. Am.*, 72:156–160, 1982.

J. Villa, I. De la Rosa, and G. Miramontes. Phase recovery from a single fringe pattern using an orientational vector-field-regularized estimator. *J. Opt. Soc. Am. A*, 22:2766–2773, 2005.